Extreme Mechanics Letters 61 (2023) 102007

Contents lists available at ScienceDirect

Extreme Mechanics Letters

journal homepage: www.elsevier.com/locate/eml

Micromechanical properties of spherical and facetted He bubble loaded copper

O. El-Atwani [a,*], J.G. Gigax [b], H. Kim [a], R.J. McCabe [a], D. Canadinc [c], M.R. Chancey [a], J. Weaver [d]

[a] Materials Science and Technology Division, Los Alamos National Laboratory, Los Alamos, NM, USA
[b] Center for Integrated Nanotechnology, Los Alamos National Laboratory, Los Alamos, NM, USA
[c] Department of Mechanical Engineering, Koc University, Istanbul, Turkey
[d] National Institute of Standards and Technology, Engineering Laboratory, Gaithersburg, MD, USA

ARTICLE INFO

Article history:
Received 23 December 2022
Received in revised form 7 March 2023
Accepted 9 March 2023
Available online 16 March 2023

Keywords:
Mechanical properties
He bubbles
Schmid factor
Shear
Ductility

ABSTRACT

Exploring new irradiation resistant materials requires understanding their mechanical responses to irradiation. Resistance to helium bubble formation and understanding bubble effects on the mechanical response of candidate materials are crucial factors to qualify materials as irradiation resistant. Here, we explore the effect of spherical and facetted helium bubbles on the mechanical response of copper via *in-situ* micromechanical tensile testing at room temperature. Bubble formation and shape effects on strength and ductility, and their behavior on grain boundaries are discussed and compared to literature. Loading Cu with helium bubbles is shown here to increase strength but decrease ductility.

Published by Elsevier Ltd.

1. Introduction

Nuclear reactor structural materials are exposed to extreme conditions and have stringent requirements on performance, safety, and stability for the duration of service life [1]. The quest to develop nuclear materials that can withstand the severe environmental conditions in future nuclear systems is an industry priority. New candidate materials should possess high resistance to morphology changes and mechanical property degradation resulting from irradiation. Among various microstructural changes, helium (He) bubble formation arising from transmutation and implantation is a prominently observed feature. These He bubbles were shown to form in irradiated materials at various conditions that affect bubble morphology and distribution in different ways [2,3]. While they can have uniform distributions in single crystalline materials, they were shown to decorate grain boundaries (GBs) in polycrystalline materials at conditions where He-vacancy defect complexes can migrate [4]. For nanoscale grain sizes, high density facetted bubbles were mainly shown to decorate GBs at relevant temperatures due to He-vacancy complex migration [5]. Furthermore, depending on the ratio of He to generated vacancies and the He pressures in the generated He bubbles, the bubble shape changes from spherical to faceted [6]. He bubbles were shown to affect the material's mechanical properties [7–11]. It is commonly believed that He bubbles can cause high temperature embrittlement in nuclear materials [11]. However, recent studies on He bubble effects on mechanical properties reveal conflicting messages. Dispersed barrier hardening and associated models correlated with nanoindentation results have demonstrated that He bubbles are moderate strength barriers that impede dislocations during deformation and cause hardening [12–14]. Ding et al. via *in-situ* transmission electron microscopy (TEM)-mechanical testing of single crystalline copper (Cu) loaded with pressurized sub-10 nm He bubbles, demonstrated that He bubbles act as dislocation sources and shearable obstacles and enhance plasticity and ductility [15]. Cunningham et al. demonstrated large softening behavior of bubble loaded ultrafine and nanocrystalline tungsten where He bubbles decorated the GBs [10]. In addition, it was recently shown that the effect of He on GBs depends on the stress state, where a decrease in yield strength was observed under tensile stress but the opposite behavior is observed under shear stress. Certain GB types might be susceptible to weakening for particular combinations of bubble morphology, bubble pressure, and/or loading conditions, and might dominate the overall mechanical response [9]. It is therefore evident that He bubble effects depend on several morphological factors including grain size due to the transition from dislocation mediated plasticity (large grain sizes) to GB mediated plasticity (grain sizes in the nanocrystalline regime) [16]. Other factors that have not been considered include bubble shape,

* Corresponding author.
E-mail addresses: oelatwan25@gmail.com, osman@lanl.gov (O. El-Atwani).

https://doi.org/10.1016/j.eml.2023.102007
2352-4316/Published by Elsevier Ltd.

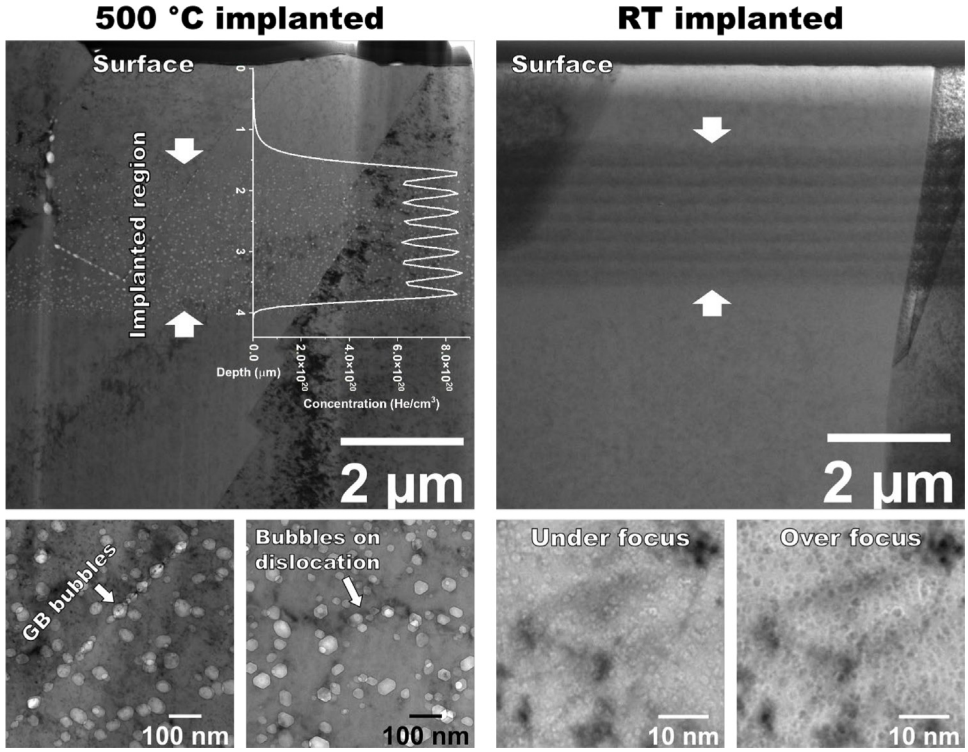

Fig. 1. Bright-field transmission electron microscope (TEM) micrographs showing Fresnel images for 500 °C and RT implanted He on Cu. He distribution profile is superimposed on the 500 °C micrograph and white arrows indicate borders of the implanted regions.

where round versus facetted bubbles may have an effect on possible He bubble shearing processes and interaction with dislocations, and the characterization methodology where nanoindentation versus micromechanical testing result in different stress states that can also affect the interpretation of results.

In this paper, we explore some of the outstanding questions on this topic. We examine the effects of bubble shape on mechanical properties using micromechanical tests on Cu samples with spherical and facetted bubbles. We use polycrystalline Cu as a model material to examine whether ductility enhancement/reduction occurs and the type of failure mode (intergranular vs intragranular) when the material is loaded with spherical or facetted He bubbles.

2. Methods

Cu samples prepared via large strain extrusion machining were recrystallized by annealing at 200 °C for 30 min. Irradiations were performed with He ions at room temperature (RT) and 500 °C. Flat-profile irradiations on recrystallized Cu at two different conditions were performed to produce uniform bubble distributions of round (RT) and facetted bubbles (500 °C). The details of the flat-profile irradiation conditions and methodology are described in the supplemental. The He depth and concentration were determined using the Stopping Range of Ions in Matter (SRIM) Monte Carlo computer code[1] (version 2013) [17] and 30 eV was used as a displacement energy. Femtosecond laser machining was used to remove part of the sample such that tensile specimens were fabricated with the gauge width and length parallel to the ion incident surface to ensure a uniform distribution of He throughout the tensile gauge thickness [18]. Micro tensile specimens were fabricated using a ThermoFisher Helios Nanolab 600 (ThermoFisher Scientific, USA) equipped with a Ga source operated at 30 kV. Successively decreasing currents from 60 nA to 5 nA were used to etch the tensile bar. A final polish was achieved using a 1 nA beam current. The nominal dimensions of the samples were 3 μm (width) × 3 μm (thickness) × 12 μm (length). Samples were characterized with a ThermoFisher Apreo scanning electron microscope (SEM) equipped with an EDAX Velocity electron backscatter detector (EBSD). Orientation mapping of all tensile specimens were characterized with EBSD, before and after testing, with 20 keV electrons and 25 nm step size.

The in-house built system, equipped with a PI-841 piezoactuator (Physik Instrumente, Germany) and a 10 mN load cell (FUTEK, USA), was used to simultaneously apply load to the tensile specimens and measure displacement. The measured displacement was corrected to a sample displacement by removing the frame compliance. All tensile data reported as engineering stress and engineering strain.

The tensile specimens were pulled at a constant displacement rate of 25 nm/s for a nominal starting strain rate lower than 2×10^{-2} 1/s. Schmid factors of the grains in the gauge lengths of the samples were calculated for the (111) [110] slip systems (slip systems in face-centered cubic (FCC) materials). All *in-situ* testing videos are found in the supplemental resources (note that SEM shows only 2D videos of the front of the samples).

3. Results

The morphologies of the irradiated samples are shown in Fig. 1 and the flat-profile He distribution is superimposed on the 500 °C morphology image. While bubbles were round and uniform for RT irradiation, the high temperature irradiation case resulted in large facetted bubbles, and the GBs were decorated with a high density of these faceted bubbles. The density and size of the bubbles were 0.23 ± 0.01 nm^{-2} and 1.8 ± 0.35 nm, respectively, for the

[1] Certain commercial equipment, instruments, or materials are identified in this paper in order to specify the experimental procedure adequately. Such identification is not intended to imply recommendation or endorsement by NIST, nor is it intended to imply that the materials or equipment identified are necessarily the best available for the purpose.

Table 1
Yield strength, ductility, Schmid factors, and fracture type in tested samples.

Sample	Yield strength (MPa) (0.2% offset)	Change in length	Schmid factors	Fracture
500 °C sample A	120	≈0.53	Grain 1 (0.5) Grain 2 (0.49)	Slip traces occurred in grain 1&2. Fracture occurred in grain 2 (intragranular)
500 °C sample B	130	≈0.4	Grain 1 (0.5) Grain 2 (0.47)	Fracture occurred in grain 1 (intragranular)
500 °C sample C	165	≈0.4	Grain 1 (0.5) Grain 2 (0.47)	Fracture occurred in grain 1 (intragranular)
RT sample A	120	≈0.4	Grain 1 (0.42) Grain 2 (0.48) Grain 3 (0.47)	Fracture occurred in grain 1 (intragranular)
RT sample B	90	≈0.4	Grain 1 (0.47) Grain 2 (0.47)	Fracture occurred in grain 1 (intragranular)
Un-implanted sample A	85	≈0.52	Grain 1 (0.43) Grain 2 (0.44) Grain 3 (0.37) Grain 4 (0.47)	Fracture occurred in grain 1 (intragranular)
Un-implanted sample B	80	≈0.43	Grain 1 (0.47) Grain 2 (0.42) Grain 3 (0.41)	Fracture occurred close to the vicinity of the grain boundary of grain 1&2

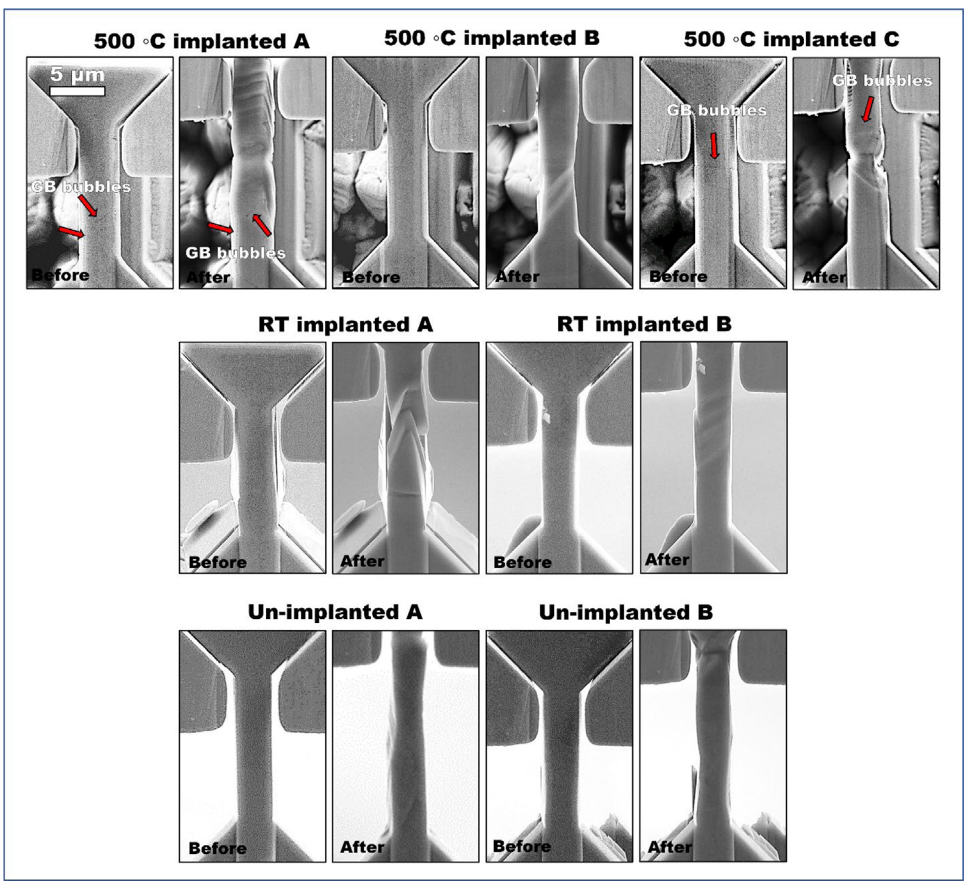

Fig. 2. Scanning electron microscopy micrographs of the tested tensile samples prior-and post-testing.

RT sample, while for the 500 °C sample the density and size of the bubbles were 0.0003 ± 0.0002 nm^{-2} and 32.7 ± 18 nm, respectively.

Three tensile samples were prepared from the 500 °C case, and two tensile samples were prepared from each of the RT irradiated and unirradiated sample cases. The morphology of the samples prior- and post-mechanical testing are demonstrated in Fig. 2, and the corresponding orientation maps showing the crystal direction normal to the sample and inverse pole figure maps showing both the crystal direction perpendicular (upper) and parallel (lower) to the tensile direction are shown in Fig. 3. The samples were purposely prepared with GBs within the gauge length and some samples had several boundaries to assess the effect of GBs on the mechanical properties. Fig. 4 provides an overview of the engineering stress strain curves of the different tensile specimens. The yield strengths, total change in length (ductility) values, Schmid factors of relevant grains, and fracture types are summarized in Table 1.

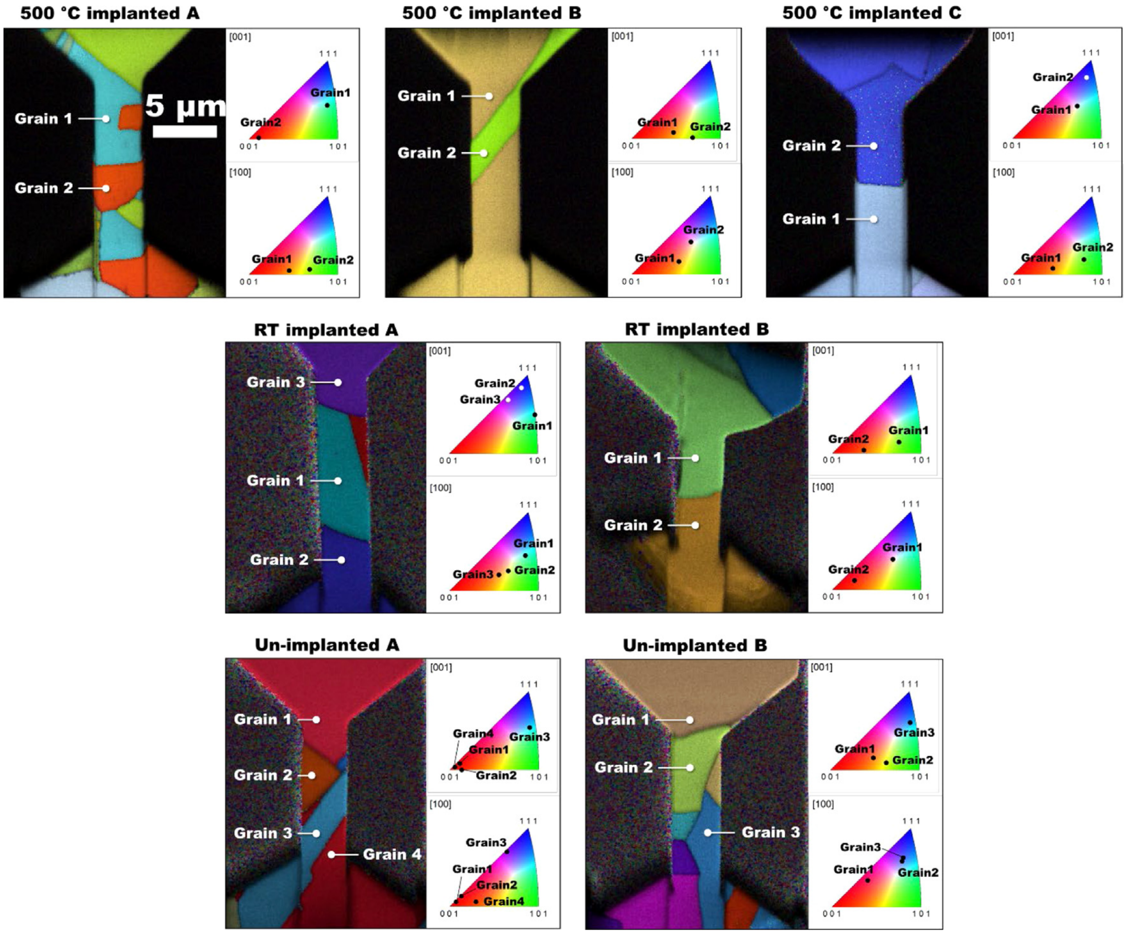

Fig. 3. EBSD orientation mapping and inverse pole figures (IPF) of the samples prior to testing. The orientation maps display the crystal direction in the sample normal direction and the inverse pole figures display the crystal direction in the sample normal (upper IPF) and applied tensile stress directions (lower IPF).

4. Discussion

The main goal of this work is to provide further results and discussion that would assist in answering several outstanding questions regarding the effect of He bubbles on the mechanical properties of materials and Cu is used as a ductile model material to satisfy this purpose. The results are also compared to relevant literature on bubble loaded materials. The goal was to answer the following questions: (1) Does softening occur for a bubble-loaded ductile material? (2) Can faceted bubbles lead to intergranular fracture? (3) Is ductility enhanced via bubble shearing? (4) Does the shape of the bubble affect the mechanical properties? (5) Do mechanical testing procedures affect the results?

All 500 °C and RT implanted samples demonstrated intragranular fractures. Even when the bubbles were facetted (500 °C implanted samples) and with an average size on the order of 10 nm, no GB fractures occurred. This contradicts behavior of facetted bubbles on brittle materials where softening [10] and embrittlement [11] is expected. Cunningham et al. demonstrated softening in ultrafine-grained tungsten loaded with facetted He bubbles [10]. He bubble formation on GBs is known to cause He bubble embrittlement, and intergranular fracture in FCC and body-centered cubic (BCC) materials, including steels [11]. The GBs in the implanted samples in the present study were mostly high angle twin boundaries, and are expected, in general, to act as strong dislocation barriers although some screw dislocations with preferred orientations can cross-slip [19]. The cross-slip mechanism on Cu (under tensile stresses), however, depends on the orientation of the dislocation, the twin surface and the Burgers vector, and has indirect mechanisms that depends on the reaction stress, where direct dislocation transformation requires a reaction stress over 400 MPa [20]. This could increase the pile up of dislocations and cause earlier fractures (mainly intergranular fractures), which did not occur. In terms of overall change in length, the implanted samples demonstrated lower values to the un-implanted samples. Except for the 500 °C implanted A sample, all other irradiated samples demonstrated 7 to 23% reduction in change in length. In terms of yield strength, all of the implanted samples demonstrated higher yield strength (up to 95% increase). There are variations among the samples implanted at the same temperature. While some of these variations can be dependent on the grain and GB orientations (Schmid factors and slip systems) and the relative GB to grain matrix ratios in these micro-sized samples, other factors are related to the effect of He bubbles in the samples. Using the dispersed barrier hardening (DBH) and associated models [12–14], He bubbles are known to induce material hardening due to bubbles acting as obstacles to dislocations. On the other hand, bubbles on the GBs can contribute to softening of the materials. Under tensile stresses, Martinez et al. [9] demonstrated through a hybrid Molecular Dynamics-Monte Carlo tool that He bubbles affect GB cohesion under tensile stresses, causing a decrease in the yield strength. Under shear, the opposite effect was observed. GBs that are inclined to the tensile direction are more complicated and the He content in the bubbles can also alter the hardening/softening behavior. The GBs in the tensile samples are mostly twin boundaries and it was shown that twin boundaries can cause strengthening or softening under micropillar compression depending on the angle between the

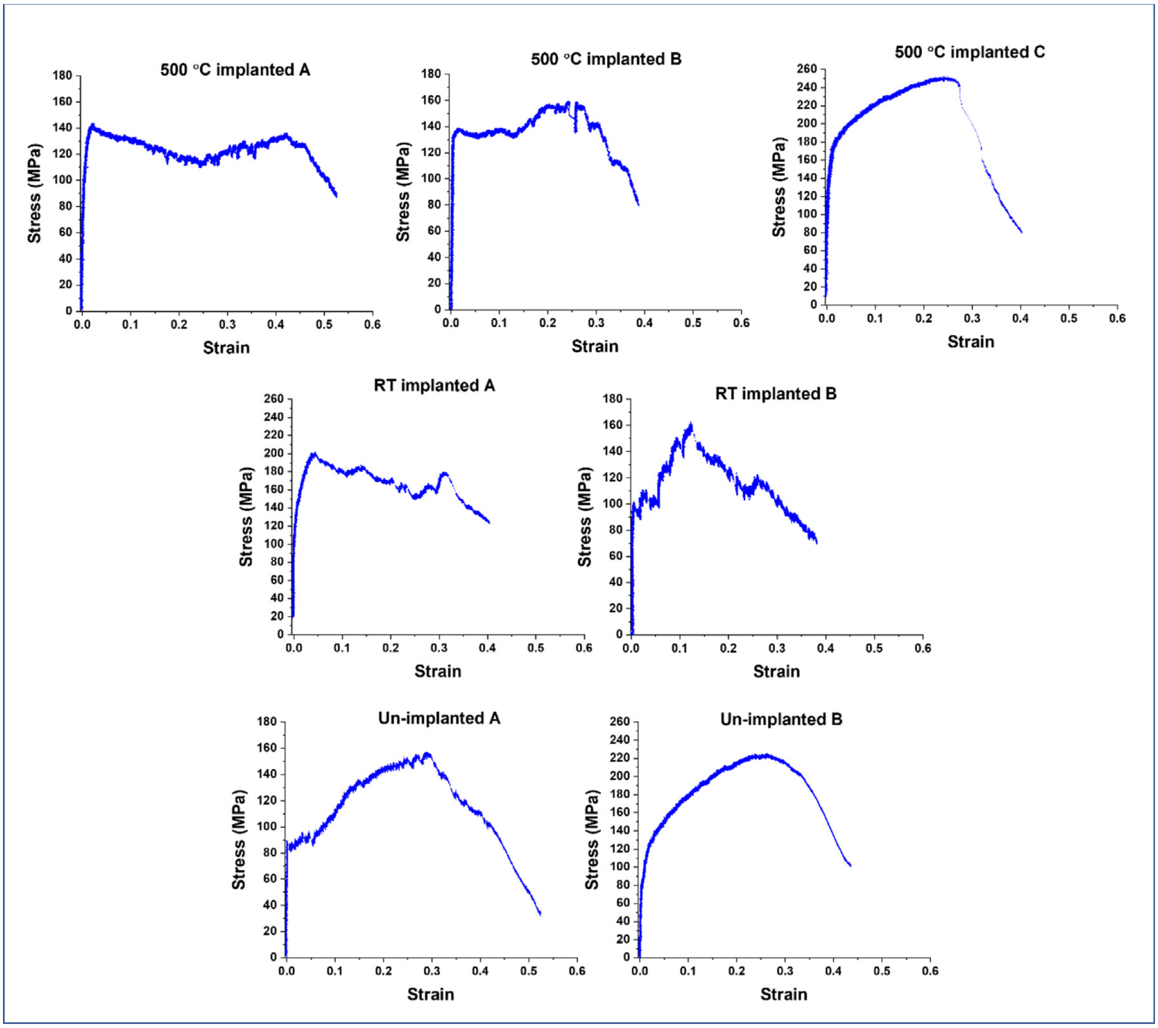

Fig. 4. Engineering stress — engineering strain curves from the microtensile tested samples.

twin boundary and the cross section of the pillar [21]. To discuss this effect under micro-tension, 3D EBSD mapping may be necessary to determine such angle. Therefore, it can be concluded that several competing hardening and softening mechanisms coexist. The microtensile samples in this work possess a low number of GBs, and thus, a complete polycrystalline effect (isotropic behavior) does not occur. In addition, the bubble behavior in different materials can be different. For example, bubbles in ultrafine W (brittle material) result in softening [10] but not for the present case in Cu. Cu is a ductile material and dislocation slip is expected. In large grain Cu, dislocation plasticity is expected, and therefore, the effect of bubbles on GBs may not alter the deformation mechanism, but pile-ups at GBs may play an important role on the fracture site. However, in W, the deformation mechanism is controlled by slow screw dislocations (screw dislocation mediated plasticity), which causes fractures to initiate on GBs [22]. Hence, the bubbles in the GBs can cause localized stresses, further decreasing the poor cohesive nature of the GBs in W due to impurities [23], resulting in another deformation mechanism (GB softening) that dominates the material's failure.

Ding et al. [15] performed *in-situ* TEM-straining experiments on single crystalline Cu. Bubbles were shown to act as shearable obstacles and dislocation sources that enhance ductility in the material. The experiments performed here are on bubble loaded Cu samples containing GBs and with less significant surface effects than in the *in-situ* TEM experiments performed by Ding et al. Our results do not indicate a ductility enhancement, but rather a decrease in ductility occurred. Ding et al. described the differences between their experiments and bulk experiments by Weibull statistics and the probability of He bubbles to link up and reach a critical size (flaw). The critical size is higher in an infinite volume (bulk material), unlike a finite volume (submicron-sized Cu single crystalline loaded with He bubbles) featured in the experiments performed by Ding et al.

Both dislocations and GBs contribute to the mechanical property results in our samples. Although He bubbles were shown to shear under mechanical stresses [15], softening from GBs and impeding dislocation motion and pile-ups near GBs can reduce ductility. Some fractures did not occur in grains with the highest Schmid factor indicating effects of GBs and dislocation pile-ups, as well as GB plasticity, on the overall strength.

When comparing the 500 °C implanted samples to the RT implanted samples, higher yield strengths are observed in the former. It is expected, via the DBH model, that the increase in hardening is proportional to barrier strength, α, and $\sqrt{Nd}$ (where N is defect density and d is defect size). $\sqrt{Nd}$ is 0.31 nm$^{-1/2}$ and 0.64 nm$^{-1/2}$ for the 500 °C and RT implanted samples, respectively (calculated from Fig. 1). Therefore, higher yield strengths are expected in the RT samples, which is not the case, indicating that α cannot be assumed to be constant if the DBH models are valid in this case. The factors that affect the barrier strength α are still not well understood [24]. This also indicates the limitation of the DBH model on complex systems where hardening and softening effects are competing. He bubbles sizes and He content can also affect bubble shearing. Liu et al. [25] demonstrated in alpha zirconium (hexagonal close-packed, HCP) that bubbles larger than 8 nm caused bubble softening, which is not the case in this work since the 500 °C had bubbles much larger than 8 nm and hardening was still observed.

Ding et al. performed their experiments in single crystalline samples where only dislocation plasticity is expected. In our work, both dislocation and GB effects coexist. Modeling and experimental works have demonstrated differences in materials' mechanical responses at different stress states. It is, therefore, evident that the experimental setup and stress state affect the conclusions deduced from these experiments. Future work should focus on ductile nanocrystalline samples where GB plasticity is expected to be the main factor affecting the material deformation behavior.

We acknowledge that our work considered cavity defects only and that dislocation loops were not considered. However, bubbles are considered defects of moderate to strong barrier strengths while dislocation loops are of weak barrier strengths [24,26,27]. Moreover, in high temperature implantation in Cu, loops are not present due to enhanced interstitial-vacancy recombination [28], and our high temperature and RT implantations demonstrated similar sample ductility, while the yield strengths were larger in the high temperature samples (where dislocation loops are not expected to be present). Therefore, it is evident that bubbles were the dominant factor affecting the mechanical behavior.

5. Conclusion

In conclusion, micromechanical tensile experiments were performed on He implanted Cu to study the effect of He bubbles on the material's mechanical properties. The tests were performed at RT and on samples with different bubble shapes. GBs existed in the gauge lengths of the specimens. Facetted bubbles were shown to produce larger hardening (yield strength) and the results are elucidated based on the DBH model. No ductility enhancements are observed. However, stronger Cu was obtained, when loaded with He bubbles, with loss in ductility. The discrepancies in yield strengths among the same temperature samples are elucidated based on the competing effects of hardening due to He bubbles, He bubble shearing and action as dislocation sources, and He bubble softening at GBs. It is also evident that the effects of bubbles are ambiguous due to the complex deconvolution of matrix and GB contributions (competing effects of hardening in the grain matrices and softening in the GBs) and the dependence on the sample morphology, experimental setups, and stress states.

Declaration of competing interest

The authors declare that they have no known competing financial interests or personal relationships that could have appeared to influence the work reported in this paper.

Data availability

The data that has been used is confidential.

Acknowledgments

This work was performed, in part, at the Center for Integrated Nanotechnologies, and office of Science User Facility operated for the U.S. Department of Energy (DOE) Office of Sciences by Los Alamos National Laboratory (Contract 89233218CNA000001) and Sandia National Laboratories (Contract DE-NA-0003525). O. E. A. acknowledges support from the Laboratory Directed Research and Development program of Los Alamos National Laboratory, USA under the early career program project number 20210626ECR.

Appendix A. Supplementary data

Supplementary material related to this article can be found online at https://doi.org/10.1016/j.eml.2023.102007.

References

[1] S.J. Zinkle, G. Was, Materials challenges in nuclear energy, Acta Mater. 61 (3) (2013) 735–758.
[2] K. Farrell, Experimental effects of helium on cavity formation during irradiation—a review, Radiat. Eff. 53 (3–4) (1980) 175–194.
[3] L. Mansur, W. Coghlan, Mechanisms of helium interaction with radiation effects in metals and alloys: A review, J. Nucl. Mater. 119 (1) (1983) 1–25.
[4] P. Lane, P. Goodhew, Helium bubble nucleation at grain boundaries, Philos. Mag. A 48 (6) (1983) 965–986.
[5] O. El-Atwani, J. Hinks, G. Greaves, et al., In-situ TEM observation of the response of ultrafine-and nanocrystalline-grained tungsten to extreme irradiation environments, Sci. Rep. 4 (2014) 4716.
[6] O. El-Atwani, W. Cunningham, D. Perez, et al., Temperature threshold for preferential bubble formation on grain boundaries in tungsten under in-situ helium irradiation, Scr. Mater. 180 (2020) 6–10.
[7] H. Ullmaier, H. Trinkaus (Eds.), Helium in metals: Effect on mechanical properties, in: Materials Science Forum, Trans Tech Publ, 1992.
[8] S.-M. Liu, S.-H. Li, W.-Z. Han, Revealing the dynamics of helium bubbles using in situ techniques, JOM 72 (6) (2020) 2352–2362.
[9] E. Martínez, B.P. Uberuaga, B.D. Wirth, Atomistic modeling of helium segregation to grain boundaries in tungsten and its effect on de-cohesion, Nucl. Fusion 57 (8) (2017) 086044.
[10] W.S. Cunningham, J.M. Gentile, O. El-Atwani, et al., Softening due to grain boundary cavity formation and its competition with hardening in helium implanted nanocrystalline tungsten, Sci. Rep. 8 (1) (2018) 2897.
[11] H. Schroeder, High temperature embrittlement of metals by helium, Radiat. Eff. 78 (1–4) (1983) 297–314.
[12] E. Nembach, Particle strengthening of metals and alloys, 1997.
[13] F. Kroupa, P. Hirsch, Elastic interaction between prismatic dislocation loops and straight dislocations, Discuss. Faraday Soc. 38 (1964) 49–55.
[14] D. Bacon, U. Kocks, R. Scattergood, The effect of dislocation self-interaction on the Orowan stress, Phil. Mag. 28 (6) (1973) 1241–1263.
[15] M.-S. Ding, J.-P. Du, L. Wan, et al., Radiation-induced helium nanobubbles enhance ductility in submicron-sized single-crystalline copper, Nano Lett. 16 (7) (2016) 4118–4124.
[16] Z. Shan, E. Stach, J. Wiezorek, et al., Grain boundary-mediated plasticity in nanocrystalline nickel, Science 305 (5684) (2004) 654–657.
[17] J.F. Ziegler, M.D. Ziegler, J.P. Biersack, SRIM–the stopping and range of ions in matter (2010), Nucl. Instrum. Methods Phys. Res. B 268 (11) (2010) 1818–1823.
[18] J.G. Gigax, H. Vo, Q. McCulloch, et al., Micropillar compression response of femtosecond laser-cut single crystal Cu and proton irradiated Cu, Scr. Mater. 170 (2019) 145–149.
[19] J. Kacher, B. Eftink, B. Cui, et al., Dislocation interactions with grain boundaries, Curr. Opin. Solid State Mater. Sci. 18 (4) (2014) 227–243.
[20] M. Chassagne, M. Legros, D. Rodney, Atomic-scale simulation of screw dislocation/coherent twin boundary interaction in Al, Au, Cu and Ni, Acta Mater. 59 (4) (2011) 1456–1463.
[21] D. Wei, M. Zaiser, Z. Feng, et al., Effects of twin boundary orientation on plasticity of bicrystalline copper micropillars: A discrete dislocation dynamics simulation study, Acta Mater. 176 (2019) 289–296.
[22] B.G. Butler, J.D. Paramore, J.P. Ligda, et al., Mechanisms of deformation and ductility in tungsten–a review, Int. J. Refract. Met. Hard. Mater. 75 (2018) 248–261.
[23] J. Morniroli, M. Gantois, M. Lahaye, Brittle fracture of polycrystalline tungsten, JMatS 20 (1) (1985) 199–206.
[24] O. El-Atwani, J. Weaver, E. Esquivel, et al., Nanohardness measurements of heavy ion irradiated coarse-and nanocrystalline-grained tungsten at room and high temperature, J. Nucl. Mater. 509 (2018) 276–284.
[25] S.-M. Liu, S.-H. Li, W.-Z. Han, Effect of ordered helium bubbles on deformation and fracture behavior of α-Zr, J. Mater. Sci. Technol. 35 (7) (2019) 1466–1472.
[26] N. Li, E. Fu, H. Wang, et al., He ion irradiation damage in Fe/W nanolayer films, J. Nucl. Mater. 389 (2) (2009) 233–238.
[27] J.S. Weaver, C. Sun, Y. Wang, et al., Quantifying the mechanical effects of He, W and He+ W ion irradiation on tungsten with spherical nanoindentation, JMatS 53 (7) (2018) 5296–5316.
[28] W. Han, E. Fu, M.J. Demkowicz, et al., Irradiation damage of single crystal, coarse-grained, and nanograined copper under helium bombardment at 450 C, J. Mater. Res. 28 (20) (2013) 2763–2770.